Interfacial gravity currents. I. Mixing and entrainment

B. R. Sutherland
Department of Mathematical Sciences, University of Alberta, Edmonton, Alberta T6G 2G1, Canada

Experiments are performed to examine mixing and transport due to an intrusive gravity current in a two- and three-layer fluid. Successive passages of the intrusion act to increase the depth of the middle layer. The observed broadening rates and the deposition of potential energy are compared with theories that neglect mixing and entrainment processes. As the middle layer widens, a transition in the mass transport by the intrusion is observed: in a two-layer fluid the intrusion transports mass along the entire length of the interface; in a three-layer fluid with sufficiently deep middle layer the intrusion transports mass over a limited distance and simultaneously excites large-amplitude internal wave modes and solitary internal waves. © *2002 American Institute of Physics.*
[DOI: 10.1063/1.1483303]

I. INTRODUCTION

Localized, rapid mixing of an interface creates a patch of fluid that ultimately gravitationally collapses into the surrounding unmixed region. One of the most dramatic observed responses to localized mixing is the occurrence of the Morning Glory.[1–4] Typically each year in the early morning hours of late October periodic bands of clouds propagate over North-Eastern Australia with widths of 4 km and spanwise extents as long as 1000 km. The south-westward propagating clouds, associated with the crests of atmospheric waves, are believed to occur in response to mixing due to sea breezes and the collision of fronts north of the Gulf of Carpentaria.[3,5,6]

Though the Morning Glory is a well-documented example, similar large-scale undular atmospheric disturbances have been observed in the mid-USA,[7] the southern United States,[8] and elsewhere (e.g., Smith *et al.*[9]). Recent Doppler radar and lidar observations have revealed the generation of undular bores from gravity currents in the form of cold thunderstorm outflows.[10,11] Indeed, such disturbances occur more frequently than satellite observations suggest. Disturbances such as Morning Glory are notable because they are made visible by clouds and they occur regularly.

An understanding of these phenomena has progressed in part by examining the collapse of a mixed region into a uniform ambient fluid.[12,13] But these studies neglect the more complicated density structure of real systems. Indeed, the process of the collapse of a localized mixed region into a stratified ambient fluid, such as a two- and three-layer fluid, is not well understood. If it is sufficiently dense, the collapsing fluid may propagate as a gravity current[14] running along a lower boundary beneath the interface. Otherwise, if the upper- and lower-layer fluids are equally mixed, the collapsing fluid may propagate along the interface itself as an intrusion. These disturbances may in turn generate bores and/or solitary waves.[15–18]

Waves and intrusions are dynamically distinguished in the way they transport mass and momentum, as illustrated schematically in Fig. 1. In Figs. 1(a)–1(d), the shaded region represents a relatively shallow layer of fluid above a rigid boundary. Figure 1(a) shows a propagating internal wave train. The net upward displacement over the wave crest equals the net downward displacement over the wave trough and therefore, to first order in amplitude, the waves transport momentum, but not mass. Figure 1(b) shows a propagating solitary wave in the form of a moving hump-like disturbance.[19] Such a nonlinear wave transports momentum and displaces mass a finite distance comparable to the horizontal extent of the wave. Figure 1(c) shows a gravity current, which transports mass and momentum long distances.[14] Finally, Fig. 1(d) shows a bore, which like a gravity current transports mass and momentum. The difference here is that the intruding fluid has the same density as the fluid into which it intrudes. In a bore, the fluid depth changes over a small distance across a hydraulic jump.

The simplest extension of shallow-water phenomena to disturbances in stratified fluid is considered in Figs. 1(e)–1(h). The diagrams draw an analogy between shallow water disturbances and disturbances in a three-layer fluid with no upper and lower boundaries. The middle layer is thin with respect to the horizontal scale of the interfacial disturbances.

Figure 1(e) shows the two types of internal waves that may be generated in a three-layer fluid: an even (sinuous) or odd (varicose) mode.[20] To first order, both waves transport momentum but not mass. By analogy with the solitary wave shown in Fig. 1(b), Fig. 1(f) shows a double-humped solitary internal wave that transports momentum and displaces mass a finite distance. The analogs of a gravity current and bore are the intrusions shown in Figs. 1(g) and 1(h), respectively.

The study of three-layer systems is of interest because they are easily described by analytic theories and they introduce dynamics that are not present in a two-layer theory. For example, the dynamic response of a three-layer fluid to an intrusion propagating along the middle layer qualitatively changes as the depth of the middle layer changes: a transition occurs in which the intrusion excites trailing large-amplitude internal waves and an interfacial solitary wave.

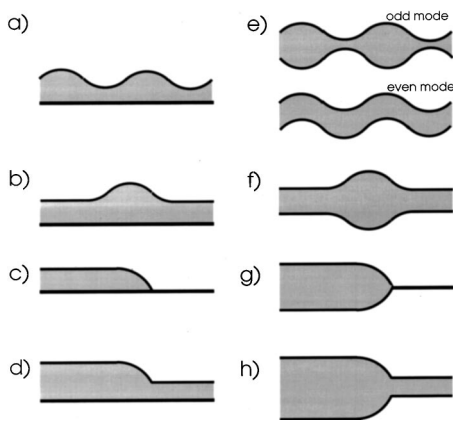This paper describes the results of a repeated series of

FIG. 1. Schematics illustrating different flow behaviors in shallow water and in a three-layer fluid with a thin middle layer: (a) internal waves, (b) solitary waves, (c) gravity current, (d) bore, (e) odd and even mode internal waves, (f) double-humped solitary wave, (g) intrusion into a two-layer fluid, and (h) intrusion into a three-layer fluid.

lock-release experiments in which an approximately two-layer fluid evolves to become an approximately three-layer fluid due to interfacial mixing resulting from the passage of successive intrusions. The focus is on the mixing and entrainment processes responsible for the broadening of the middle layer.

The deepening of a turbulent mixing region that overlies a denser static fluid has been examined in "mixing-box" experiments.[21–23] Measurements of the entrainment velocity (the speed at which the interface between the two fluids deepens) have been shown to have a power law dependence on the Richardson number, which is a measure of the stability of the stratified flow. The results of mixing-box experiments can be only qualitatively compared with measurements of entrainment rates across an interface by an intrusion: in the latter case, the entrainment occurs impulsively rather than continuously.

The experimental setup and analytic techniques are described in Sec. II. In Sec. III analytic functions are matched to the observed density profiles. The broadening of the middle layer and the energy redistribution are examined in Sec. IV. Section V describes the qualitative change in behavior of an intrusion as it propagates first into a two-layer fluid and then, from run to run, into a three-layer fluid with successively increasing middle-layer thickness. Conclusions are summarized in Sec. VI.

II. EXPERIMENTAL SETUP

For most of the results reported upon here, the experiments are performed in a rectangular acrylic tank of length $L=180$ cm, width 10 cm, and depth 20 cm. A metal clip is inserted halfway along the top of the tank to reduce the bowing of the sidewalls when the tank is filled with fluid. As a result, the width of the tank changes by no more than 1 mm over its length. A schematic of the initial setup is shown in Fig. 2(a). The tank is filled initially to 8.5 cm depth with salt water of density ρ_1. Fresh water, of density ρ_0, is then layered on top through a sponge float until the total depth of fluid in the tank is 17 cm. A thin gate is inserted near one end

of the tank to form a lock of length $\ell \ll L$. Foam insulating tape is fastened around the edges of the acrylic gate in order to prevent leakage of fluid from one side of the gate to the other.

Once the gate is firmly in place, the fluid in the lock is well mixed until its density is uniform. Because the two layers of fluid in the tank have approximately equal depth, the resulting density of fluid in the lock is $\rho_m \simeq (\rho_0 + \rho_1)/2$.

Accurate measurements of the ambient density profiles, $\bar{\rho}(z)$, are found using a conductivity probe that is attached to a computer-controlled vertical traverse mechanism. Eight salt solutions of different densities ranging from that of distilled water to 1×10 g/cm^3 are used to calibrate the probe. The probe is hooked up to a computer which digitizes the signal at a frequency of 100 Hz. The density profile is found by passing the probe vertically downward through the fluid between 3 and 14 cm depth. Except for brief acceleration and deceleration times, the probe moves at a constant speed of 1 cm/s. While the probe is moving the computer simultaneously records both the probe position and digitized conductivity. The probe calibration data are used to transform the voltage signal at each depth to a measure of density, and a Gaussian weighted averaging technique is used to smooth the result. The standard deviation is taken to be 0.5 cm. Finally, to correct for electronic drift in the signal from the probe, the profiles are rescaled to ensure that mass is conserved, i.e., the density at the top and bottom are fixed and the value of each integrated density profile is constant between runs. A check on the reliability of these measurements is also provided using a refractometer and two or three drops of fluid sampled from the probe tip at the top and bottom of the traverse.

Dye is added to the fluid in the lock in order to visualize the transport of this fluid after the gate is removed. Mylar paper is fastened along the rear wall of the tank and fluorescent lights are suspended above the tank. A camera is positioned far from the tank with its lens level with the interface of the initial (approximately) two-layer fluid. The camera is 350 cm from the tank and is oriented with the lens at the position of the gate. Its field of view is set to visualize the tank between 1 and 159 cm from the lock end of the tank. The signal from the camera is recorded on SVHS tape and is simultaneously digitized on a computer using the image processing language, DigImage.[24] The resulting data are used to measure the structure and speed of transport of the fluid released from the lock. The dyed fluid also enables interfacial waves to be visualized.

A single experiment is comprised of several individual runs. In the first run the tank is filled with an approximately two-layer fluid, as described previously, and propagation of fluid in the lock is monitored after the gate is released. The fluid is found to propagate along as an intrusion, as has been observed in earlier studies.[15,16] The system is allowed to evolve to a steady state, in which the fluid in the tank is stationary, as shown schematically in Fig. 2(b). A conductivity probe is then traversed vertically through the fluid to measure the resulting density profile.

To set up for the second run, the gate is reinserted, as before, a distance ℓ from the end of the tank. The fluid in the
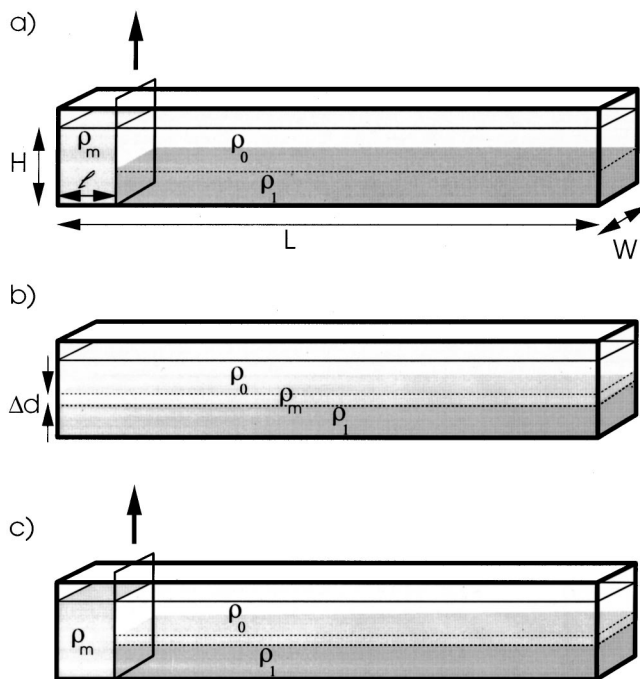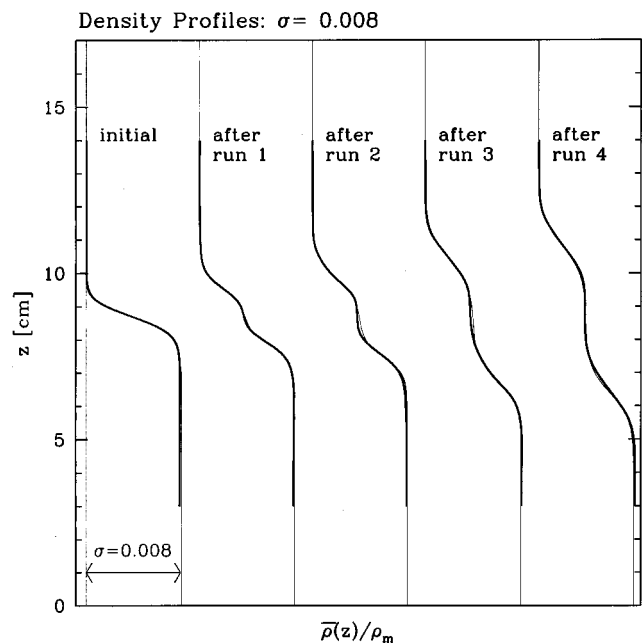
FIG. 2. Setup of lock-release experiment.

FIG. 3. Measured density profiles (heavy lines) between successive runs of experiment A. The light lines are analytic approximations to measurements.

lock is remixed and a different dye is added to this fluid: By symmetry, the resulting density of fluid in the lock is ρ_m as in the case of the first run. However, the fluid along the length of the tank outside the lock has a different density profile due to the mixing along the interface. During the second run the gate is removed and the fluid in the lock collapses as it intrudes into the modified background stratified fluid, as shown schematically in Fig. 2(c).

The process is repeated in successive runs: the system is allowed to approach steady state; the density profile is measured with a conductivity probe; the gate is reinserted at the same position; the fluid in the lock is dyed and mixed so that it has uniform density ρ_m; the gate is then pulled out and a camera records the propagation of the intrusion into the ambient stratified fluid. The experiment ends after the density of the fluid 1 cm from the top or bottom of the fluid changes non-negligibly due to mixing.

As a result of successive mixing along the interface, a transition is typically observed: in early runs the intrusion extends to the end of the tank; in late runs the intrusion propagates a limited distance along the tank and internal and solitary waves are generated.

III. DENSITY PROFILES

A. Observations

Two experiments are reported upon in detail in this section. In what will be referred to hereafter as "experiment A," the initial density difference between the upper and lower layers of the approximately two-layer fluid is relatively small. Explicitly, $\sigma \equiv \Delta \rho / \rho_m \simeq 0.008$ where $\Delta = \rho_1 - \rho_0$. In "experiment B" the initial relative density difference is more than four times larger: $\sigma \simeq 0.036$. In both experiments, the lock length $\ell = 12.5$ cm.

Figure 3 shows the density profiles from successive runs in experiment A. The heavy lines show the data determined from the vertically traversed conductivity probe. The data measured between successive runs are horizontally offset, but the density scale for each is the same. The diagram clearly shows that, as a result of successive mixing by the intrusion, the approximately two-layer fluid becomes an approximately three-layer fluid: after run 4, the fluid in the tank is stratified with three well-defined regions of uniform density.

Corresponding to each density profile are profiles of the squared buoyancy frequency, N^2 [for a Boussinesq fluid, $N^2 = -(g/\rho_m)d\bar{\rho}/dz$], which are plotted in Fig. 4. The scale for each plot is the same, ranging from 0 to 5 s^{-2}. After run 4, the fluid at the mean depth of the fluid is unstratified, bounded above and below by two stratified "interfaces." The maximum buoyancy frequency decreases between successive runs and the width of the interface thickens.

Similarly, in experiment B the ambient density changes from a two-layer to three-layer fluid between successive runs. Figures 5 and 6 show the density and N^2 profiles, respectively, over a series of runs. A uniform intermediate layer develops between the upper and lower layers and the thickness of this layer widens by approximately the same degree between runs as in the corresponding cases in experiment A.

The most apparent difference between the two cases is the asymmetry of the profiles for the runs in experiment B. In particular, examination of the N^2 profiles shows that the upper interface is less broad and more strongly stratified than the lower interface. This is a consequence of the fact that the initial mean depth of the interface (where N^2 is greatest) is moderately above $z = 8.5$ cm, the mean depth of the tank. Thus when the fluid in the lock is mixed, the mean density of this fluid is moderately greater than the density at the mean

Phys. Fluids, Vol. 14, No. 7, July 2002
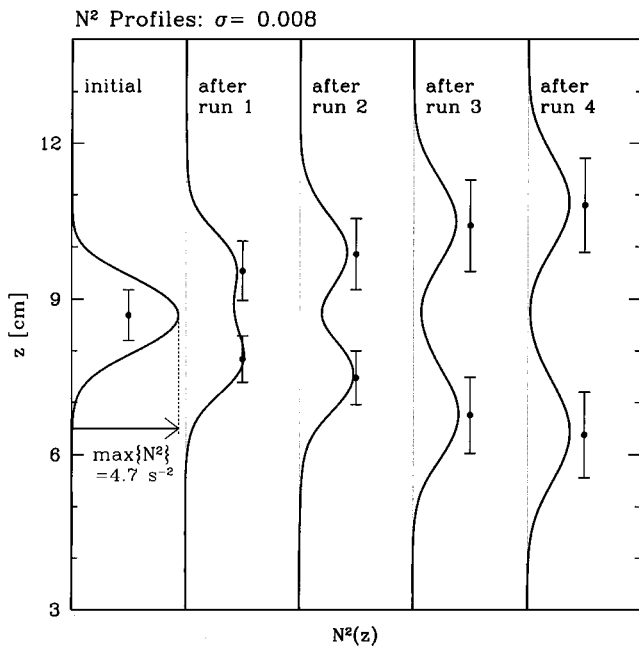
Interfacial gravity currents   2247

FIG. 4. Squared buoyancy frequency profiles between successive runs of experiment A. The bars indicate the calculated position and width of the interfaces.
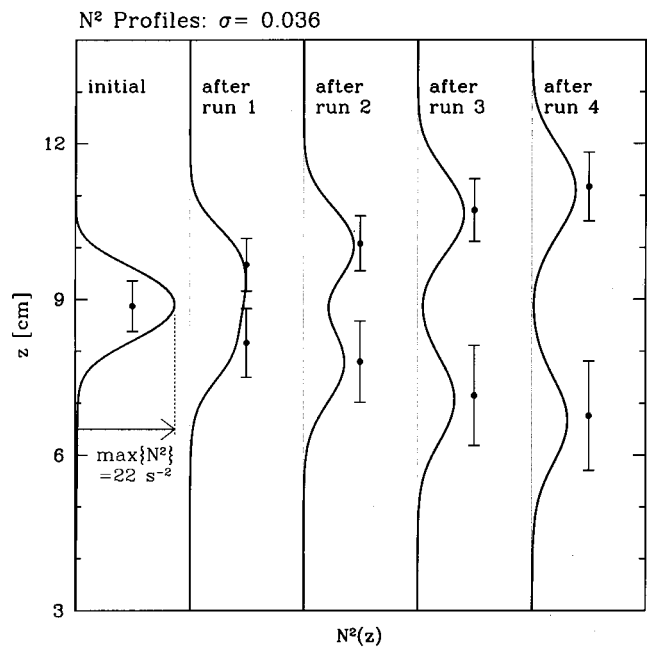
depth of the interface. When the gate is released the mean depth of the intrusion is below the mean depth of the interface and so mixes the upper and lower interfaces differently.

B. Analysis

The following analysis has been employed to characterize the manner in which the density structure evolves between different runs in each experiment. It is assumed that the experimentally determined profile $\bar{\rho}(z)$ can be represented analytically by

FIG. 5. As in Fig. 3 but for experiment B.

FIG. 6. As in Fig. 4 but for experiment B.

$$\bar{\rho}_{\text{thy}}(z) = \rho_0 + \frac{1}{4}\Delta\rho\left[1 - \tanh\left(\frac{z-z_u}{D_u}\right)\right]$$
$$+ \frac{1}{4}\Delta\rho\left[1 - \tanh\left(\frac{z-z_l}{D_l}\right)\right], \tag{1}$$

in which z_u and z_l are the mean depths of the interfaces above and below the middle layer, respectively, and D_u and D_l are their corresponding thicknesses. The initial density profile is represented by setting $z_u = z_l \equiv z_0$ and $D_u = D_l \equiv D_0$, in which case

$$\bar{\rho}_{\text{thy}}(z) = \rho_0 + \frac{1}{2}\Delta\rho\left[1 - \tanh\left(\frac{z-z_0}{D_0}\right)\right]. \tag{2}$$

Values of ρ_0 and Δ are fixed, and z_u, z_l, D_u, and D_l are determined from a (nonlinear) least-squares fit. Specifically, an initial guess is made for these four quantities and the following sum is computed:

$$S = \sum_{i=1}^{N} (\rho(z_i) - \bar{\rho}_{\text{thy}}(z_i))^2, \tag{3}$$

in which the sum is taken over the N samples of the experimentally determined profile. Typically $N=111$, corresponding to samples equally spaced by 1 mm between 3 and 14 cm depth.

To minimize S with respect to z_u, the sum in Eq. (3) is then computed twice more for fractionally larger and smaller values of z_u. Quadratic curves are then fit to the results; that is, the coefficients a, b, and c are determined so that $S = a(z_u)^2 + b(z_u) + c$ holds for each of the three pairs of data. An estimate of the value of z_u that minimizes S is given by $z_u \simeq -b/2a$.

Likewise, the values of z_l, D_u, and D_l that minimize S are also estimated. This procedure is then repeated iteratively until z_u, z_l, D_u, and D_l converge to values accurate to three
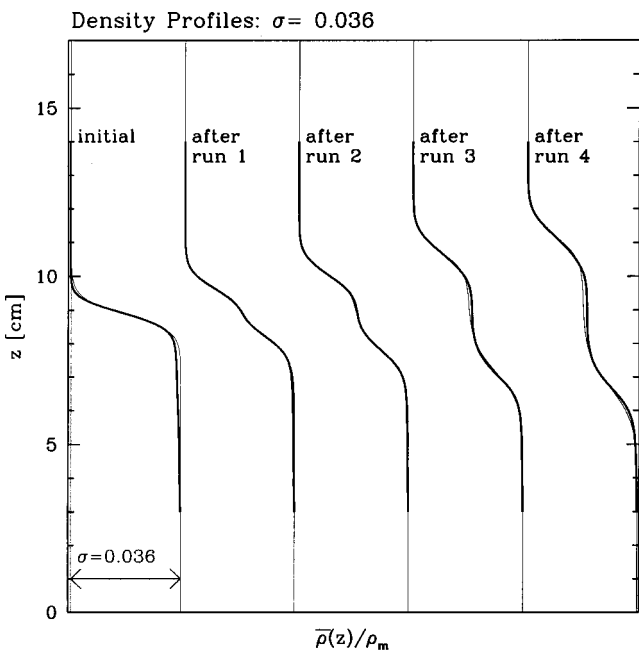
TABLE I. Variations in the characteristics of density profiles after successive runs of two experiments. Values of z_u, z_l, D_u, and D_l in cm.

Expt.	Run	z_u	z_l	D_u	D_l	Error
A	Initial	8.69		0.49		0.008
	Run 1	9.54	7.84	0.57	0.45	0.016
σ: 0.008	Run 2	9.86	7.48	0.68	0.52	0.035
	Run 3	10.41	6.76	0.88	0.73	0.055
	Run 4	10.80	6.38	0.91	0.82	0.074
B	Initial	8.87		0.49		0.12
	Run 1	9.67	8.16	0.51	0.66	0.023
σ: 0.036	Run 2	10.08	7.80	0.53	0.78	0.017
	Run 3	10.72	7.15	0.60	0.96	0.091
	Run 4	11.17	6.76	0.66	1.05	0.18

significant digits. This numerical convergence procedure proved to be more efficient than attempts to find zeros of S/z_u, etc.

Table I lists values of z_u, z_l, D_u, D_l calculated in this manner for several runs of experiments A and B. The last column in Table I gives the error, defined by min$\{S\}/\sigma^2$, where σ is the calculated standard deviation of the experimental data. In the two experiments, as in experiments with up to 10 runs, the error is found to increase with run number.

In a separate analysis, in which the density profiles were matched to the "error function" (erf(z)) instead of hyperbolic tangent functions, the iterative procedure produced comparable values of z_u and z_l and the associated error min$\{S\}/\sigma^2$ was comparable for run numbers greater than 2. For early runs, and especially for a two-layer fluid, the hyperbolic tangent functions fit more accurately to the observed density profiles.

The first experiment listed corresponds to the density profiles shown in Fig. 3. In Fig. 3, the theoretically determined profiles calculated using (1) with the parameters given in Table I are, respectively, superimposed on the experimentally determined profiles. The corresponding mean position of the interfaces and their widths are illustrated in Fig. 4. The closed circles are plotted at the depths of center of the interfaces, and the vertical bars extend from $z_u - D_u$ to $z_u + D_u$ at the upper interface and from $z_l - D_l$ to $z_l + D_l$ at the lower interface.

The greatest shift in the position of the interface occurs during the first run. The single interface broadens and may be represented by the superposition of two interfaces displaced upward and downward by approximately 0.8 cm. In successive runs thereafter the upper and lower interfaces are displaced by approximately 0.4 cm between runs. The widths of the two interfaces broadens by approximately 0.1 cm between successive runs. In these experiments the upper layer is wider than the lower layer by approximately 0.1 cm.

In experiment B, the mean position of the interface is initially 0.2 cm closer to the surface than in the first experiment, and is approximately 0.4 cm above the mean depth of the fluid in the tank. As a result of this asymmetry, when the fluid in the lock is mixed the resulting density is greater than the mean $\rho_m = 1.0165$ g/cm^3 by 0.0009 g/cm^3. Between successive runs the upper and lower interfaces are displaced by approximately the same degree as the corresponding runs of

the first experiment. However, the width of the lower layer broadens at approximately twice the rate of the upper layer. Thus, independent of the density difference, the intrusion acts to separate the layers to the same degree but mixes the lower layer to a greater extent.

In experiments with very small density differences ($\sigma < 0.005$) we find the density profiles develop a more complicated structure than a three-layer fluid. Figure 7 shows the scaled density profiles taken after the tenth run of four experiments each with $H = 17$ cm and $\epsilon = 0.043$ but with different σ. For $\sigma = 0.0019$ and 0.0032 the profiles develop multiple steps, which are more pronounced with weaker stratification. For $\sigma > 0.005$ the fluid is well characterized by a three-layer fluid. This critical value of σ is found to be approximately the same in experiments with $H = 34$ cm and in experiments with $\epsilon = 0.094$. The reason for this change in dynamics is an interesting separate study in itself: as is obvious from observing the transport of dyed intrusions released from the lock into weakly stratified fluid, during late runs the collapsing fluid in the lock forms two intrusions that
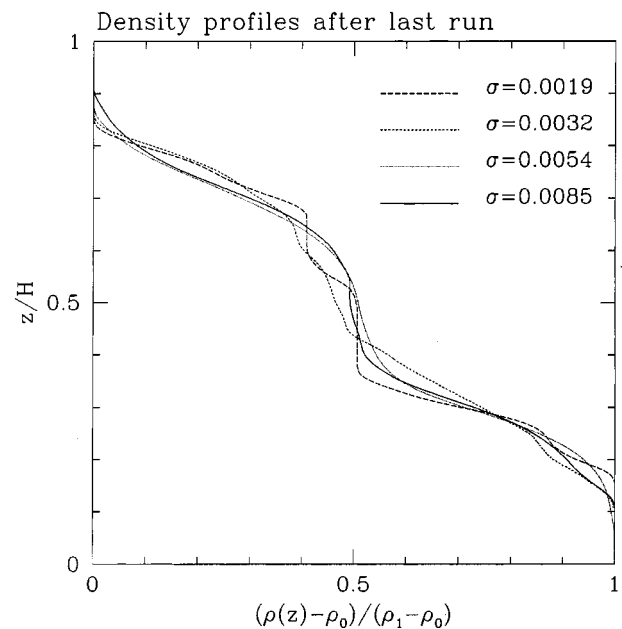

FIG. 7. Scaled density profiles measured in the last ($N = 10$) run of four experiments with $H = 17$ cm, $\epsilon = 0.043$ and for the indicated values of σ.

move individually along the upper and lower interfaces of the middle layer.

A detailed analysis of these dynamics is beyond the scope of this paper. However, preliminary evidence suggests that the transition occurs when the time scale for collapse of the lock fluid is slower than the time scale for mixing over the extent of the lock.

IV. MIXING AND ENTRAINMENT

The structure of the density profiles and their associated energy over successive runs may be compared with theoretical predictions that neglect mixing and entrainment processes. In this way we may assess the relative importance of these processes to the broadening of the middle layer and the stored available potential energy.

A. Middle layer width

The depth of the middle layer may be estimated by computing $z_u - z_l$, as described in Sec. III. However, for the purposes of modeling entrainment processes, it is better to define the depth as the separation distance between two isopycnal surfaces above and below the intrusion. Somewhat arbitrarily, we consider the depth of two isopycnal surfaces with densities $\rho_+ = (\rho_0 + \rho_m)/2$ and $\rho_- = (\rho_1 + \rho_m)/2$. Defining $z_\pm = \bar{\rho}^{-1}(\rho_\pm)$, the middle layer depth is thus given by $z_+ - z_-$.

In a theory that neglects mixing processes, we assume that the entire volume of uniform fluid in the lock before run N slumps into a horizontal layer of uniform density after the run. By conservation of mass, the change of thickness of this layer is

$$\Delta d \equiv d_N - d_{N-1} = (H - d_{N-1})\epsilon, \qquad (4)$$

where d_N is the depth of the middle layer after run N, and $\epsilon = \ell/L$ is the ratio of the lock length to tank length. Solving the recursion formula (4) one finds

$$d_N = H[1 - (1-\epsilon)^N] + d_0(1-\epsilon)^N. \qquad (5)$$

For small values of ϵ and N, the middle layer depth is predicted to increase linearly with N: $d_N \simeq d_0 + (H - d_0)N$.

In reality the intruding fluid not only separates the upper and lower layers but, as the lock fluid intrudes into the middle layer, it entrains fluid across the upper and lower isopycnal surfaces at $z = z_+$ and z_-, respectively.

Figure 8 shows that, for a variety of experiments, the increase in width of the middle layer is well predicted by Eq. (5). The squares denote the measured values of $z_+ - z_-$. The error associated with these measurements is estimated to be 0.5 cm. The initial width of the interface is taken to be $d_0 = z_+ - z_-$ evaluated before the first run.

The agreement is best in strongly stratified fluid experiments, characterized by relative density difference $\sigma = 0.023$. The agreement is good whether the lock length is small ($\epsilon = 0.043$) or long ($\epsilon = 0.094$) [as shown in Figs. 8(a) and 8(d), respectively], and the agreement is good whether the middle interface is thin ($d_0 = 0.57$ cm) or thick ($d_0 = 1.9$ cm) [as shown in Figs. 8(a) and 8(c), respectively].
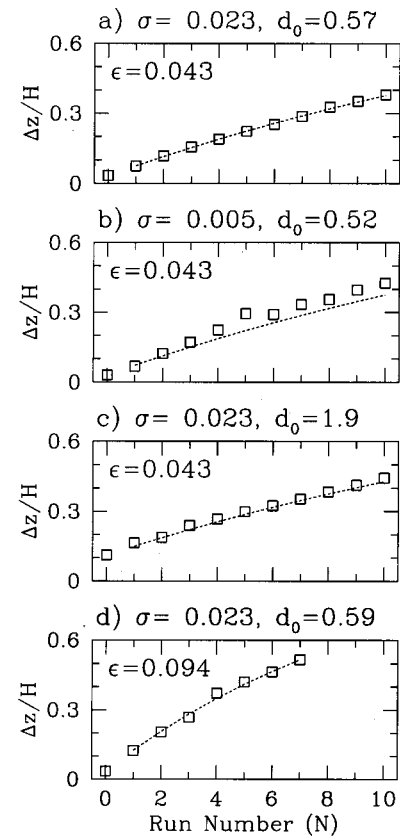

FIG. 8. Observed increase in the width of the middle layer (squares) compared with a theoretical prediction (dashed line) which neglects mixing and entrainment processes. The four experiments are characterized as indicated by the relative density difference σ, initial interface thickness, d_0, and the aspect ratio, ϵ of the lock to tank length.

For the experiment whose results are shown in Fig. 8(c), the relatively diffuse interface is established by filling the tank with a two-layer fluid as usual and then waiting 20 h before running the experiment. As a result of molecular diffusion, the initial interface is over three times thicker than the corresponding thin interface case in Fig. 8(a).

In Fig. 8(b), the results are shown for a weakly stratified experiment with relative density difference approximately one-fifth that of the corresponding strongly stratified case in Fig. 8(a). The middle layer depth is found to broaden at a moderately greater rate than predicted by Eq. (5). Thus weakly stratified intrusions entrain fluid more efficiently across the isopycnal surfaces as the lock fluid collapses.

If the middle-layer width is measured by $z_u - z_l$, the above-mentioned qualitative results hold for late runs. However, the results are ambiguous during early runs when the middle-layer width is comparable to the thickness of the interface of the initial two-layer fluid.

In order to characterize the relative broadening rate of the middle layer, we perform a regression analysis to determine the value ϵ_d in Eq. (5) which gives the best fit to the experimental data between runs $N = n_0$ and n_f. Specifically, ϵ_d is the value of ϵ that minimizes
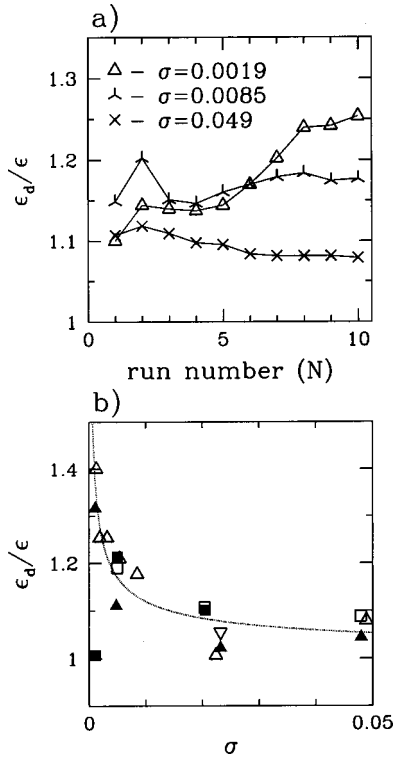
$$\sum_{n=n_0}^{n_f} (\Delta z - d_n)^2,$$

FIG. 9. (a) Ratio to ϵ of best-fit value, ϵ_d, determined between runs 0 and N in three experiments with $H=17$ cm, $\epsilon=0.043$, and σ as shown. (b) Values of ϵ_d/ϵ vs σ in 18 experiments with $H=17$ cm and $\epsilon=0.043$ (open triangles), $H=17$ cm and $\epsilon=0.094$ (closed triangles), after run $N=10$, and with $H=34$ cm and $\epsilon=0.043$ (open squares), $H=34$ cm and $\epsilon=0.094$ (closed squares) after run $N=5$. The upside-down open triangle corresponds to an experiment with an initially thick interface, $d_0=1.9$. The best-fit power law curve through the points is represented by the dotted line.

where Δz is the observed width of the middle layer after run N, and d_N is given by (5). As such, ϵ_d represents the effective relative lock length that would best reproduce the observed broadening of the middle layer between runs n_0 and n_f. This regression analysis is necessary to average the effect of variations between individual runs of the observed density profile characteristics.

Figure 9(a) shows relative values of ϵ_d as determined in three experiments with $H=17$ cm, $\epsilon=0.043$ and for weak, moderate, and strong stratifications as characterized by σ. The points show values of ϵ_d/ϵ measured from a regression analysis taken for data between runs $n_0=0$ and $n_f=N$. In general, for $\sigma>0.005$, ϵ_d varies by less than 10% as N increases: the broadening rate does not depend upon the number of intrusions. For $\sigma<0.005$, ϵ_d increases by as much as 20% as N increases. This is a consequence of the more complicated density structure that develops in weakly stratified fluid, as shown in Fig. 7.

Figure 9(b) plots values versus σ of ϵ_d/ϵ as determined between runs 0 and 10 in experiments with $\epsilon=0.043$ cm and between runs 0 and 5 in experiments with $\epsilon=0.094$ cm. The upper bound for the latter regression analysis is chosen so that ϵN is approximately the same in all cases. Different symbols indicate different experimental parameters: open (closed) symbols are drawn for experiments with lock

lengths characterized by $\epsilon=0.043$ (0.094) and triangles (squares) are drawn for $H=17$ cm (34 cm).

In all cases $\epsilon_d/\epsilon>1$. Thus more fluid is entrained into the middle layer as a result of the collapse of fluid in the lock and the ensuing mixing that occurs on either flank of the propagating intrusion. The plot demonstrates that, unless $\sigma<0.005$, the degree of entrainment depends upon σ and not upon H or ϵ. From the best-fit power-law curve through the data [the dotted curve in Fig. 9(b)], we find $\epsilon_d/\epsilon \simeq 1 + (\sigma/\sigma_0)^p$, in which $\sigma_0=0.000\,152\pm0.000\,005$ and $p=-0.505\pm0.09$. This relationship is less reliable for $\sigma<0.005$.

B. Available potential energy

When the fluid in the lock is mixed, available potential energy is stored which is partially converted to kinetic energy after the gate is extracted and the lock-fluid released. The kinetic energy is ultimately lost due to viscous dissipation and redeposition of potential energy as a result of mixing above and below the intrusion. In order to characterize this energy loss, the change of potential energy during a run is compared with the initial available potential energy.

After run N the potential energy of the fluid per unit width of the tank is

$$\mathrm{PE}_N=L\int \bar{\rho}_N(z)gz\,dz, \tag{6}$$

where $\bar{\rho}_N$ is the measured density profile after run N and, for convenience, $\bar{\rho}_0$ denotes the initial density profile.

The potential energy of the fluid is greatest when the fluid is so well mixed that it is homogeneous. In this case the resulting density is $\langle\rho\rangle=(\int\rho_N(z)dz)/H\simeq\rho_m$ and the potential energy is

$$\mathrm{PE}_{\max}=L\langle\rho\rangle gH^2/2. \tag{7}$$

The available potential energy of a particular run is defined to be the maximum energy that can be lost or stored by vertically rearranging fluid parcels. After run N, the available potential energy is given explicitly by

$$\mathrm{APE}_N=\mathrm{PE}_{\max}-\mathrm{PE}_N. \tag{8}$$

In particular, the maximum available potential energy in a given experiment is $\mathrm{APE}_0=\mathrm{PE}_{\max}-\mathrm{PE}_0$.

As a measure of the potential energy permanently stored between successive runs due to mixing and entrainment, we compute the nondimensional ratio

$$R_N\equiv\frac{\mathrm{APE}_0-\mathrm{APE}_N}{\mathrm{APE}_0}=\frac{\mathrm{PE}_N-\mathrm{PE}_0}{\mathrm{PE}_{\max}-\mathrm{PE}_0}, \tag{9}$$

which is an increasing function with values between 0 and 1.

Before a run energy is stored by mixing the fluid in the lock, so that the total potential energy per unit width in the tank is $\mathrm{PE}_N^{\mathrm{pre}}=\ell\langle\rho\rangle gH^2/2+(1-\epsilon)\mathrm{PE}_{N-1}$, and the corresponding available potential energy is

$$\mathrm{APE}_N^{\mathrm{pre}}=(1-\epsilon)[\mathrm{PE}_{\max}-\mathrm{PE}_{N-1}]=(1-\epsilon)\mathrm{APE}_{N-1}, \tag{10}$$

and therefore

Phys. Fluids, Vol. 14, No. 7, July 2002

Interfacial gravity currents   2251

$$R_N^{\text{pre}} = R_{N-1} + \epsilon \frac{\text{APE}_{N-1}}{\text{APE}_0}. \qquad (11)$$

That is, mixing the fluid in the lock increases the relative stored available potential energy by an amount $\epsilon \text{APE}_{N-1}/\text{APE}_0$.

Upon releasing the gate, this energy is converted to kinetic energy which in turn irreversibly deposits potential energy along the length of the tank as a result of the broadening of the middle-layer depth and thickening of the interfaces above and below the middle layer. The relative amount of energy which is permanently deposited after run N is $R_N < R_N^{\text{pre}}$.

The observed energy deposition can be compared with a theory that neglects mixing and entrainment processes. We assume that the experiment starts with a two-layer fluid (with $d_0 = 0$) and that between successive runs the lock fluid slumps into the middle layer to form a uniform slab of fluid. Thus, after run N the middle layer depth is d_N, as given by Eq. (5).

In a theory that neglects mixing (i.e., analyzing the potential energy change between successive piecewise-constant density profiles of two- and three-layer fluids), it is a simple matter to show that $\text{PE}_N = \text{PE}_0 + L/8\langle\rho\rangle g(d_N)^2$, and that

$$R_N^{(\text{thy})} = \left(\frac{d_N}{H}\right)^2 = [1 - (1-\epsilon)^N]^2. \qquad (12)$$

Note that $R_N^{(\text{thy})}$ is independent of the density difference between the upper and lower layers. For small ϵ and N, $R_N^{(\text{thy})} \simeq N^2 \epsilon^2$.

The relative available potential energy in the tank before a run is predicted to be

$$R_N^{\text{pre(thy)}} = \left(\frac{d_{N-1}}{H}\right)^2 + \epsilon\left[1 - \left(\frac{d_{N-1}}{H}\right)^2\right]$$

$$= 1 - 2(1-\epsilon)^N + (1-\epsilon)^{2N-1}. \qquad (13)$$

For small ϵ and N, $R_N^{\text{pre(thy)}} \simeq \epsilon^2 + (N-1)^2 \epsilon^2$.

During a run, even neglecting mixing and entrainment, the stored potential energy in the lock is inevitably lost as the intrusion propagates along the tank. The loss is greatest during early runs as measured by $R_N^{\text{pre(thy)}} - R_N^{(\text{thy})} = \epsilon(1 - \epsilon)^{2N-1}$.

The theoretical predictions are compared with four different experiments in Fig. 10. For each run, crosses and squares denote experimentally determined values of R_N^{pre} and R_N, respectively. The error associated with these measurements is estimated to be 0.01. In each plot, values of $R_N^{\text{pre(thy)}}$ and $R_N^{(\text{thy})}$ are illustrated by dotted and dashed lines, respectively.

As anticipated, the theoretical predictions underestimate the actual stored potential energy: the stored potential energy in the lock fluid is partially redeposited due to mixing and entrainment processes. Comparing Figs. 10(a) and 10(b), two experiments with the same lock length and approximately the same initial interface thickness, but with different relative densities, σ, more energy is found to be redeposited if σ is large.
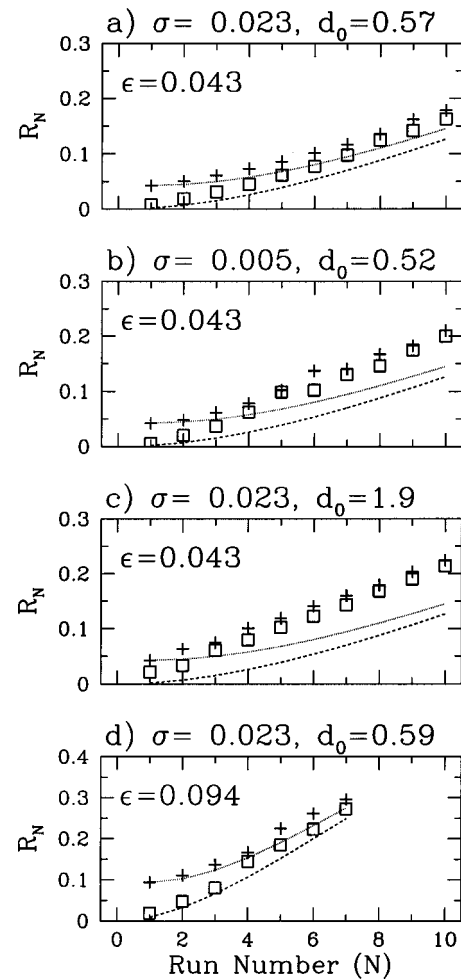

FIG. 10. Observed increase in the stored available potential energy over a number of runs in four experiments as indicated by values of σ, d_0 and ϵ (as in Fig. 8). Crosses denote the measured relative available potential energy before each run (after the fluid in lock is mixed), and squares denote this energy after each run. The observations are compared with the theoretical predictions of the relative available potential energy before (dotted line) and after (dashed line) each run. The theory neglects mixing and entrainment processes.

Though perhaps counterintuitive, these results are consistent with tilted tank experiments,[25] which examine interfacial mixing in stratified shear flows. These show that mixing is enhanced if the stratification is large. This can be explained in theory by examining the properties of the Richardson number, which is a measure of the stability of a stratified shear flow.[26] Typically flows are dynamically unstable if the Richardson number is less than unity. The Richardson number is proportional to the density gradient divided by the square of the shear. Tilted tank experiments reveal that larger density gradients allow proportionally stronger shear, and therefore the Richardson number decreases with increasing stratification.

Likewise, in our experiments, the intrusion propagates more rapidly in strongly stratified fluid and so, because the Richardson number is small, more mixing occurs as a result of dynamic instability of the upper and lower flanks of the fluid.

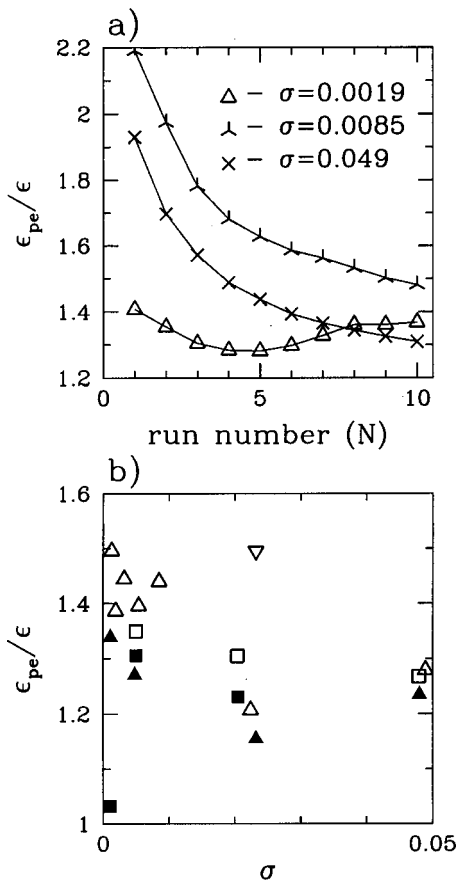As in Fig. 9, Fig. 11 shows the analysis of the change in

FIG. 11. As in Fig. 9, but for ratio of ϵ_{pe} to ϵ.

available potential energy relative to that predicted by a theory that neglects mixing. Specifically, Fig. 11 shows values of ϵ_R/ϵ, where ϵ_R is the value of ϵ that minimizes

$$\sum_{n=n_0}^{n_f} (R_n - R_n^{(thy)})^2,$$

in which $n_0=0$ and $n_f=N$. These are determined in three experiments with $H=17$ cm and $\epsilon=0.043$.

R_N measures the relative increase in potential energy (and, hence, a relative decrease in available potential energy) between successive runs, and $R_N^{(thy)}$, given by (12), measures the theoretical increase in the absence of mixing. If $\epsilon_R/\epsilon > 1$, the net potential energy in the tank increases at a faster rate than that which can be attributed to the potential energy of the lock-fluid alone. Thus the loss of available potential energy serves not only to broaden the width of the middle layer but also to thicken the extent of the upper and lower interfaces.

Indeed, in all experiments ϵ_R/ϵ is significantly greater than one, and, for $\sigma > 0.005$, this ratio decreases by as much as 30% as N increases. This occurs because, for small values of N, R_N tends to increase with nonzero slope, whereas theory predicts that R_N is proportional to ϵN for ϵ and N sufficiently small. The comparison between experiment and theory improves as the best-fit curves is fit over a greater range of run numbers.

Figure 11(b) shows values of ϵ_R/ϵ as determined between runs 0 and $N=10$ for experiments with $\epsilon=0.043$ and between runs 0 and $N=5$ for experiments with $\epsilon=0.094$. The plot shows that $\epsilon_R/\epsilon \simeq 1.3 \pm 0.2$. Generally, the ratio tends to decrease as sigma increases although the results of two experiments act against this trend. In one case, the fluid is weakly stratified ($\sigma=0.001, H=34$ cm, $\epsilon=0.094$) and the density profile at late runs deviates significantly from a three-layer fluid. In the second case, the initial interface thickness $d_0=1.9$ cm is approximately three times wider than the other experiments. In this case the R_N increases linearly even for small N [e.g., see Fig. 10(c)] and so the approximately quadratic best fit curve given by $R_N^{(thy)}$ is a poor fit to data.

The ratio ϵ_R/ϵ is generally smaller in experiments with $\epsilon=0.094$, however this is in part an artifact of the smaller range over which the regression fit is found. If, for data from experiments with $\epsilon=0.094$, we find ϵ_R from a regression fit between 0 and $N=4$, the values of ϵ_R/ϵ more closely correspond to those found in experiments with $\epsilon=0.043$.

Nonetheless, we expect moderately smaller values of ϵ_R/ϵ in experiments with longer locks because, for large intrusions or wide middle layers, less available potential energy is ultimately employed to entrain fluid across the upper and lower interfaces. Instead, the energy is lost due to viscous dissipation of the kinetic energy within the middle layer.

Interestingly, ϵ_R/ϵ is only a weak function of the relative density difference σ.

Thus available energy is consumed by a comparable amount but its use is partitioned differently: as a result of entrainment in a weakly stratified fluid more available potential energy in the lock is redeposited as potential energy along the length of the tank; in a strongly stratified fluid more energy is lost to viscous dissipation.

V. INTRUSION STRUCTURE

Images of the released lock-fluid as it propagates along an interface may be used to estimate the mass and momentum transport. Here the images are used to draw the qualitative distinction between an intrusion that transports mass long distances in the form of an interfacial gravity current (in a two-layer fluid), and one that transports this mass only a short distance in a three-layer fluid.

Although the middle layer becomes successively wider from run to run, it is not always the case that the fluid from the lock is evenly distributed along the length of the tank: during the first run, the fluid in the lock is transported to the end of the tank; after three or four runs, the fluid in the lock is found to intrude only a fraction of the distance along the tank, and large-amplitude waves are generated.

The transport of fluid along the interface of an approximately two-layer fluid is shown by the sequence of frames in Fig. 12. The frames are taken every 15 s during the first run of experiment A. In each diagram the left-hand side of the box corresponds to the position near the lock at $x \simeq 14$ cm,
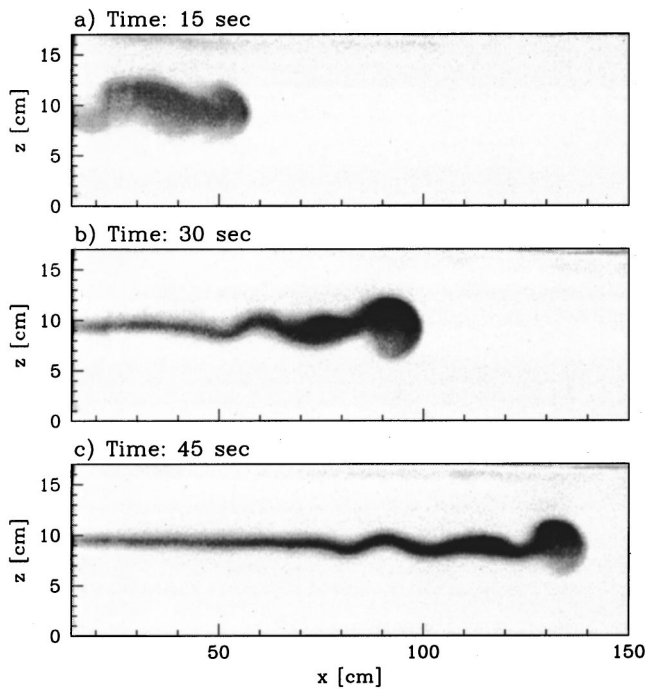
FIG. 12. Propagation of an intrusion in a two-layer fluid (first run of experiment A).

FIG. 13. Propagation of an intrusion in a three-layer fluid (fourth run of experiment A).

and the right-hand side corresponds to a position 150 cm from the lock-end of the tank.

The lock fluid, visualized by dye, propagates along the interface while depositing fluid there due to irreversible mixing. The head of the current is larger than the trailing flow. Unlike the typically observed behavior of a dissipative gravity current over a free slip bottom boundary,[13] here a trailing train of internal waves is generated. In this run the horizontal wavelength of the internal waves is approximately 15 cm and they persist for two wavelengths behind the head of the intrusion. The phase speed of the waves is moderately slower than the intrusion speed.

Over longer times the intrusion reflects from the right wall of the tank and propagates back along the interface, enhancing the mixing there further. The intrusion propagates back and forth over approximately three tank lengths before its motion is no longer discernible.

The mass transport of fluid in the lock as it intrudes into an approximately three-layer fluid is significantly different. Figure 13 shows the propagation of fluid released from the lock in run 4 of experiment A. The background three-layer fluid is visualized by a successive series of horizontal dye lines. The fluid in the lock is dark-colored as it intrudes along this interface. The obvious difference between runs 1 and 4 is that in the latter run the fluid in the lock intrudes only as far as 95 cm from the lock-end of tank. To the right of this position a double-humped interfacial solitary wave is excited. This propagates without significant change in form until it reflects from the right end of the tank.

Trailing the solitary waves are quasiperiodic interfacial waves. The amplitude of these waves is larger than that observed in run 1, and the number of waves is greater. For a bottom-propagating gravity current, Benjamin[13] argued that
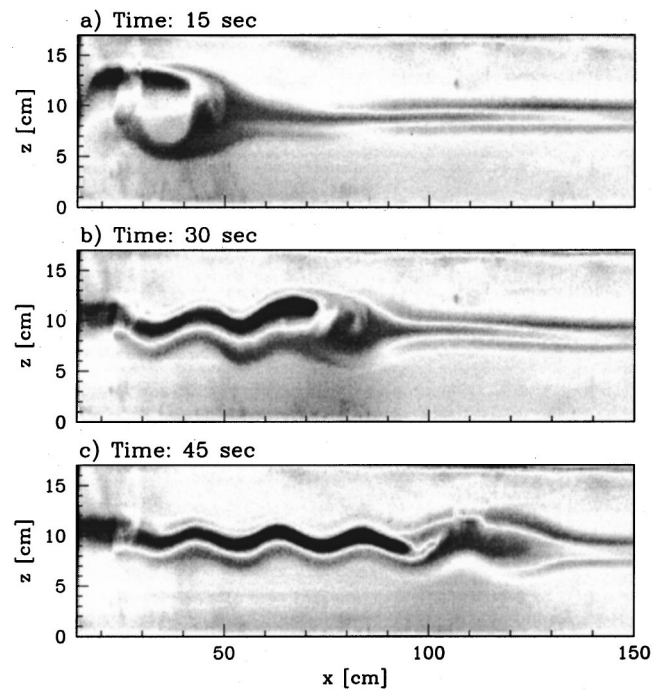
the trailing flow behind the gravity current head must be supercritical and so trailing waves could not occur. In a three-layer fluid, by symmetry, the same arguments would preclude the excitation of trailing odd-mode internal waves (see Fig. 1). However, even-mode (sinuous) waves, which are in fact observed, may be permitted because such waves do not significantly change the width of the middle layer as they oscillate through one phase. The introduction of moderately complex stratification therefore introduces qualitatively new dynamics. The flow associated with solitary and internal waves is observed to be laminar. Thus entrainment is expected to be larger in early runs of experiments (when the middle-layer depth is small) because the intrusion acts to entrain fluid as it propagates along the entire length of the tank.

VI. CONCLUSIONS

Successive intrusions have been shown to mix an interface so that an approximately two-layer fluid becomes a three-layer fluid. In response to this change, a transition occurs in the dynamics of the collapsing mixed region from one that transports mass long distances to one that transports mass a short distance but still transports momentum long distances. The momentum is transported by a double-humped interfacial solitary wave.

The theory and analysis presented here aims to characterize the relevant parameters that control the broadening of the middle layer. It is found that the middle layer broadens at a rate given at lowest order by a theory that neglects mixing and entrainment. The broadening rate (and hence, the rate of entrainment of surrounding fluid into the middle layer) is greater if the fluid is more weakly stratified.

The data suggest an empirical relation between the observed and predicted expansion rate of the form $\epsilon_d/\epsilon \sim 1 + (\sigma/\sigma_0)^{-1/2}$. That is, between successive intrusions entrainment acts to increase the middle layer depth by a factor

$$\Delta d_{\text{entrain}} \propto \epsilon/\sqrt{\sigma}. \tag{14}$$

The mixing rate, as characterized by the relative increase in potential energy over successive runs, generally decreases as σ increases but shows no consistent dependence on H or ϵ. It does depend upon the middle-layer depth, however. For moderately broad middle-layer depths, R_N tends to increase linearly rather than quadratically as predicted by a theory that neglects mixing.

In adapting this study to a realistic geophysical fluid system, there are many more degrees of complication that must be considered. The system studied here is almost symmetric about middepth in the tank. Despite this, we observe asymmetry in the density profiles as they develop between runs. We attribute this to the slight departures from perfect symmetry of the initial density profile. The inherent asymmetry of the lock-release mechanism (the lock is always pulled upwards) and the difference between the upper (free-slip) and lower (no-slip) boundary conditions may also play a role, though these effects should be minor if the middle layer depth is small and the lock is rapidly extracted. Future studies will examine these effects together with response of the system to successively more asymmetric initial density profiles and lock-fluid densities.

ACKNOWLEDGMENTS

[1] R. H. Clarke, "The Morning Glory: An atmospheric hydraulic jump," J. Appl. Meteorol. **11**, 304 (1972).

[2] D. R. Christie, K. J. Muirhead, and R. H. Clarke, "Solitary waves in the lower atmosphere," Nature (London) **293**, 46 (1981).

[3] J. C. Clarke, R. K. Smith, and D. G. Reid, "The Morning Glory of the Gulf of Carpentaria: An atmospheric undular bore," Mon. Weather Rev. **109**, 1726 (1981).

[4] A. Menhofer, R. K. Smith, M. J. Reeder, and D. R. Christie, " 'Morning-Glory' disturbances and the environment in which they propagate," J. Atmos. Sci. **54**, 1712 (1997).

[5] R. H. Clarke, "Colliding sea-breezes and the creation of internal atmospheric bore waves: Two-dimensional numerical studies," Austr. Meteorol. Mag. **31**, 207 (1984).

[6] J. A. Noonan and R. K. Smith, "Sea breeze circulations over Cape York Peninsula and the generation of Gulf of Carpentaria cloudlike disturbances," J. Atmos. Sci. **43**, 1679 (1986).

[7] S. Haase and R. K. Smith, "Morning Glory wave clouds in Oklahoma: A case study," Mon. Weather Rev. **112**, 2078 (1984).

[8] J. C. Clarke, "Picture of the month: An atmospheric undular bore along the Texas coast," Mon. Weather Rev. **126**, 1098 (1998).

[9] R. K. Smith, N. Crook, and G. Roff, "The Morning Glory: An extraordinary atmospheric undular bore," Q. J. R. Meteorol. Soc. **108**, 937 (1982).

[10] R. Fulton, D. S. Zrnic, and R. J. Doviak, "Initiation of a solitary wave family in the demise of a nocturnal thurderstorm density current," J. Atmos. Sci. **47**, 319 (1990).

[11] S. E. Koch, P. B. Dorian, R. Ferrare, S. H. Melfi, W. C. Skillman, and D. Whiteman, "Structure of an internal bore and dissipating gravity current as revealed by Raman lidar," Mon. Weather Rev. **119**, 857 (1991).

[12] G. H. Keulegan, "An experimental study of the motion of saline water from locks into fresh water channels," Technical Report No. 5168 Nat. Bur. Stand. Rept. (1957).

[13] T. B. Benjamin, "Gravity currents and related phenomena," J. Fluid Mech. **31**, 209 (1968).

[14] J. E. Simpson, *Gravity Currents*, 2nd ed. (Cambridge University Press, Cambridge, 1997).

[15] T. Maxworthy, "On the formation of nonlinear internal waves from the gravitational collapse of mixed regions in two and three dimensions," J. Fluid Mech. **96**, 47 (1980).

[16] R. E. Britter and J. E. Simpson, "A note on the structure of the head of an intrusive gravity current," J. Fluid Mech. **112**, 459 (1981).

[17] J. W. Rottman and J. E. Simpson, "The formation of internal bores in the atmosphere: A laboratory model," Geotech. Test. J. **115**, 941 (1989).

[18] R. Manasseh, C.-Y. Ching, and H. J. S. Fernando, "The transition from density-driven to wave-dominated isolated flows," J. Fluid Mech. **361**, 253 (1998).

[19] P. G. Drazin, *Solitons* (Cambridge University Press, Cambridge, 1983).

[20] P. G. Drazin and L. N. Howard, "Hydrodynamic stability of parallel flow of inviscid fluid," Adv. Appl. Math. **9**, 1 (1966).

[21] H. Rouse and J. Dodu, "Turbulent diffusion across a density discontinuity," La Houille Blanche **10**, 530 (1955).

[22] J. S. Turner, "The influence of molecular diffusivity on turbulent entrainment across a density interface," J. Fluid Mech. **33**, 639 (1968).

[23] J. S. Turner, *Buoyancy Effects in Fluids* (Cambridge University Press, Cambridge, 1973).

[24] S. B. Dalziel, "Rayleigh-Taylor instability: Experiments with image analysis," Dyn. Atmos. Oceans **20**, 127 (1993).

[25] S. A. Thorpe, "Experiments on the instability of stratified shear flows: Miscible fluids," J. Fluid Mech. **46**, 299 (1971).

[26] P. G. Drazin and W. H. Reid, *Hydrodynamic Stability* (Cambridge University Press, Cambridge, 1981).